The importance of ceramide headgroup for lipid localisation in skin lipid models

Beddoes, C.M.; Gooris, G.S.; Barlow, D.J.; Lawrence, M.J.; Dalgliesh, R.M.; Malfois, M.; ... ; Bouwstra, J.A.

The importance of ceramide headgroup for lipid localisation in skin lipid models

Charlotte M. Beddoes [a], Gert S. Gooris [a], David J. Barlow [b], M. Jayne Lawrence [b], Robert M. Dalgliesh [c], Marc Malfois [d], Bruno Demé [e], Joke A. Bouwstra [a,*]

[a] *Division of BioTherapeutics, Leiden Academic Centre for Drug Research, University of Leiden, Leiden, the Netherlands*
[b] *Division of Pharmacy and Optometry, Manchester University, Manchester, United Kingdom*
[c] *ISIS Neutron and Muon Source, Science and Technology Facilities Council, Rutherford Appleton Laboratory, Harwell Oxford, Didcot OX11 0QX, United Kingdom*
[d] *ALBA Synchrotron, Carrer de la Llum 2-6, 08290 Cerdanyola del Valles, Barcelona, Spain*
[e] *Institut Laue-Langevin, Grenoble, France*

ABSTRACT

The stratum corneum's lipid matrix is a critical for the skin's barrier function and is primarily composed of ceramides (CERs), cholesterol (CHOL) and free fatty acids (FFAs). The lipids form a long periodicity phase (LPP), a unique trilayer unit cell structure. An enzyme driven pathway is implemented to synthesize these key lipids. If these enzymes are down- or upregulated as in inflammatory diseases, the final lipid composition is affected often altering the barrier function. In this study, we mimicked down regulation of enzymes involved in the synthesis of the sphingosine and CER amide bond. In a LPP lipid model, we substituted CER N-(tetracosanoyl)-sphingosine (CER NS) with either i) FFA C24 and free sphingosine, to simulate the loss of the CER amide bond, or ii) with FFA C24 and C18 to simulate the loss of the sphingosine headgroup. Our study shows the lipids in the LPP would not phase separate until at least 25% of the CER NS is substituted keeping the lateral packing and conformational ordering unaltered. Neutron diffraction studies showed that free sphingosine chains localized at the outer layers of the unit cell, while the remaining CER NS head group was concentrated in the inner headgroup layers. However, when FFA C18 was inserted, CER NS was dispersed throughout the LPP, resulting in an even distribution between the inner and outer water layers. The presented results highlight the importance of the CER NS headgroup structure and its interaction in combination with the carbon chain invariability for optimal lipid arrangement.

1. Introduction

The barrier function of the skin is essential for terrestrial life; it prevents both the penetration of external substances and water loss from within [1]. This barrier is maintained by the outermost layer of the skin, the stratum corneum (SC). This layer is composed of corneocytes embedded in an extracellular lipid matrix [2]. The lipid matrix forms the only continuous structure through the SC and is therefore a key component of the barrier function [3,4].

The major lipid classes in the SC's extracellular lipid matrix are ceramides (CERs), cholesterol (CHOL) and free fatty acids (FFAs). In healthy SC, these lipids are present in an approximately equi-molar ratio. The SC lipids form two co-existing lamellar structures with repeat distances of ~13 and ~6 nm, referred to as the long and short periodicity phases (LPP and SPP) [5–7] respectively. These phases maintain a dense lipid packing, primarily an orthorhombic phase, but with smaller lipid subpopulations packed in the lesser dense hexagonal and fluid phases [8,9]. Both the lamellar organization and lipid density are critical for an optimal barrier function [10] and are sensitive to the

lipid composition. The LPP is a unique structure only found in the SC. It is a centrosymmetric trilayer lamellar structure, where the lipid subclasses localize within particular sublayers [11].

The lipids in the SC are obtained primarily by de novo synthesis at the epidermis [12]. The de novo synthetic pathway of the lipids in the matrix is controlled by a series of enzymes. The downregulation of enzymes can affect the final composition of SC lipids, and this can seriously compromise the lipid packing and barrier function. A key group of enzymes in this pathway are ceramide synthases, which are responsible for the attachment of the acyl chain to the sphingoid base to create the twin-chained N-acyldihydrosphingosine, which is a precursor to CERs. The ceramidase enzymes have the reverse function, cleaving the CER amide bond and producing a sphingoid base and fatty acid products that are involved with the desquamation of the skin [13]. Ceramidase is found upregulated in aged skin [14], and bacteria-derived ceramidase is linked with atopic dermatitis [15,16]. The activity of ceramide synthases and ceramidase, therefore, can change the ratio of sphingosine and FFAs in comparison with CERs in healthy SC.

In this study, we sought to investigate the effect on the LPP structure

---

of a reduced CER concentration, due to enhanced degradation or inhibited synthesis, by mimicking the downregulation of enzymes involved in the de novo synthesis of SC lipids. A simple LPP model was used to compare the lamellar organization, lateral packing, and lipid localization. In this system CER N-(tetracosanoyl)-sphingosine (CER NS) was partially substituted with FFA C24 and free sphingosine C18 (Sphingo-sub), to investigate the CER amide bond's relevance for the lipid arrangement within the unit cell of the LPP (Fig. 1). Then, to further examine the importance of headgroup moiety for the LPP lipid arrangement and stability, a similar model was prepared wherein CER NS was partially substituted with FFA C24 and FFA C18 (FFA-sub). We show that there are no changes in the lateral packing or lamellar organization when up to 25% of the non-acyl CER NS is substituted with either variant; there are differences seen in the lipid loci, however, with the free sphingosine tails locating primarily in the outer layers of the LPP unit cell. We show too that in the FFA-sub model, the FFA C18 does not localize to a particular region within the unit cell, and this results in a more even distribution of the CER NS head group between the inner and outer water regions of the LPP. The significance of these observations with respect to the LPP stability is discussed.

2. Materials and methods

2.1. Materials

Synthetic linoleate esterified omega-hydroxyacyl-sphingosine (CER EOS C30), and N-(tetracosanoyl)-sphingosine (CER NS C24) with sphingoid chain lengths of C18, were all kindly donated by Evonik, Essen, Germany. CER nomenclature was used based on the definitions from Motta et al. [17]. Stearic acid (C18), lignoceric acid (C24), cholesterol (CHOL) and D_2O (99.9%) were purchased from Sigma-Aldrich Chemie GmbH, Schnelldorf, Germany. Partially deuterated CER NS (CER NS-d7), and partially deuterated free sphingosine (sphingosine-d7), were deuterated at the three-terminal carbons of the sphingosine chain, while deuterated FFA C18 (FFA C18-d35), was deuterated along the entire acyl chain. Both the d7 and d35 deuterated lipids were purchased from Avanti Polar Lipids, Alabama, USA. The partially deuterated CER NS (CER NS-d47) was deuterated along the entire acyl chain and was kindly provided by Evonik, Essen, Germany. All solvents used were of analytical grade and supplied by Labscan, Dublin, Ireland. The water was of Millipore quality produced by a Milli-Q water filtration system with a resistivity of 18 MΩ cm at 25 °C. Nucleopore polycarbonate membranes, with 0.05 μm pore size were purchased from Whatman, Kent, UK.

2.2. Lipid matrix models

The lipid composition used as our model comprised CER EOS, CER NS, CHOL and FFA C24 in a 0.4:0.6:1:1 molar ratio and mimics several aspects of the lipid organization in the SC, including the formation of the LPP and a primarily orthorhombic lateral packing. This composition mimics the lamellar organization and lateral behaviour of more complex models while remaining simple enough for clear data interpretation [18]. The CER EOS concentration was increased from native concentrations (around 12%) to 40 mol% of the CER content, to ensure the LPP would form exclusively [19,20]. This elevation does not affect the LPP's

structure [19].

The lipid composition was then changed by substituting a single CER NS with a FFA C24 and either free sphingosine (x% Sphingo-sub) or FFA C18 (x% FFA sub), with x representing the percentage of CER NS substituted. In all models, the carbon chain number and length remained consistent. For the small angle neutron scattering (SANS) measurements, CER NS-d7, CER NS-d47, FFA C18-d35 and sphingosine-d7 were substituted into the model, replacing their protiated counterparts. A complete list of samples with lipid composition are present in Table 1.

2.3. X-ray diffraction measurements

A total of 1 mg of the desired lipid composition was prepared in chloroform:methanol (2:1 v/v) to a concentration of 5 mg/mL. This was sprayed at 14 μL/s onto polycarbonate membranes under a steady stream of nitrogen over an area of 1 × 3 mm, using a y-axis adapted Camag Linomat IV sample applicator (Muttenz, Switzerland). Samples were equilibrated at 85 °C for 30 min and then cooled to room temperature. Samples were hydrated in an oxygen-free, 84% relative humidity environment for 5 days at room temperature.

Small-angle X-ray diffraction (SAXD) measurements were performed at the NCD-SWEET beamline at the ALBA synchrotron (Barcelona, Spain). The wavelength was set at 0.999 Å. The Pilatus 1 M detector was set at a distance of 2.148 m from the sample, and had a pixel array of 981 × 1043, with each pixel being 172 × 172 μm². The experimental setup was calibrated with silver behenate. The samples were measured for 20 s at 23 °C. The one-dimensional intensity profiles were obtained by integrating from the beam centre over a 90° segment. Samples were measured in duplicate. Peak position was fitted with a Pearson7 function in Fityk [21], and the repeat distance (d) was determined through least square fitting.

2.4. FTIR measurements (Varian)

Samples were prepared with a method similar to that described in Section 2.3, but with 1 mg of sample sprayed onto a AgBr window, over an area of 10 × 10 mm. Samples were hydrated in a 100% humidity

Table 1
Model compositions used in this study.

| Model	Composition	Ratio
0% Sub	CER EOS:CER NS:CHOL:FFA C24	0.4:0.6:1:1
25% Sphingo-sub	CER EOS:CER NS:Sphingosine:CHOL:FFA C24	0.4:0.45:0.15:1:1.15
50% Sphingo-sub	CER EOS:CER NS:Sphingosine:CHOL:FFA C24	0.4:0.3:0.3:1:1.3
75% Sphingo-sub	CER EOS:CER NS:Sphingosine:CHOL:FFA C24	0.4:0.15:0.45:1:1.45
100% Sphingo-sub	CER EOS:Sphingosine:CHOL:FFA C24	0.4:0.6:1:1.6
25% FFA-sub	CER EOS:CER NS:FFA C18:CHOL:FFA C24	0.4:0.45:0.15:1:1.15
50% FFA-sub	CER EOS:CER NS:FFA C18:CHOL:FFA C24	0.4:0.3:0.3:1:1.3
75% FFA-sub	CER EOS:CER NS:FFA C18:CHOL:FFA C24	0.4:0.15:0.45:1:1.45
100% FFA-sub	CER EOS:FFA C18:CHOL:FFA C24	0.4:0.6:1:1.6
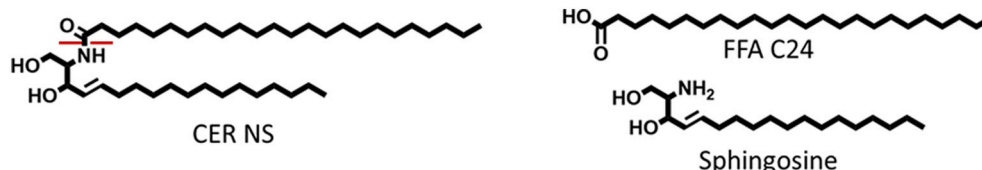
Fig. 1. Schematic of CER NS (left) split along the amide bond (red dashed line) to form FFA C24 (top right) and sphingosine (bottom right).

environment in deuterated acetate buffer (pH = 5) at 37 °C for >15 h. FTIR spectra were measured with a Varian Bio-Rad Excalibur FTIR spectrometer (Cambridge, MA), combined with a liquid nitrogen cooled broad-band mercury cadmium telluride detector. During measurements, air moisture was purged with dry air. Data were collected at a resolution of 1 cm^{-1} by the coaddition of 256 spectra over 4 min. Samples were measured over a wavenumber range of 500–4000 cm^{-1}. The thermotropic behaviour was measured in the range of 10–100 °C at a 1 °C interval, resulting in a heating rate of 0.25 °C/min. The spectra were deconvoluted using the full-width half-maxima value of 4 cm^{-1} and an enhancement factor of 1.7. Data were processed with Agilent resolution pro (Agilent Technologies, CA, USA). Linear regression fitting was used to determine the mid-transition temperature. Samples were measured in duplicate.

2.5. Neutron diffraction measurements

2.5.1. Sample preparation

Neutron diffraction samples were prepared by a method similar to that described above, but with 10 mg of lipids prepared and sprayed onto a silicon wafer over an area of 40 × 13 mm. Samples were equilibrated at 70–75 °C for 30–60 min to ensure lipid chain melting while preventing lipid film contraction and were then cooled back to room temperature. Before measuring, the samples were hydrated in D_2O/H_2O mixtures at ratios of 100:0, 50:50 and 8:92 (v/v) in 100% relative humidity, initially for ~18 h, at 32 °C. Once measured, samples were hydrated to the next water ratio for at least 8 h at 32 °C, to ensure complete solvent exchange within the LPP.

2.5.2. Measurements at LARMOR

The lipid arrangement when 25% of the CER NS in the model was substituted with sphingosine and FFA C24 (25% Sphingo-sub), was measured with the time-of-flight SANS Larmor instrument at the ISIS neutron and muon source (Rutherford Appleton Laboratory, UK). Samples were measured using neutrons with wavelengths of $1 \leq \lambda \leq 13$ Å at a fixed incident angle of 2.5°. The incoming beam size was 1 × 30 mm, while the ^{3}He tube detector was set at a 2θ angle of 5° at a distance of 4.4 m from the sample. The detector covers an area of 664 × 600 mm with a pixel size of 4 × 8 mm. The SANS patterns were normalized for the profile of the incident wavelength spectrum using a measurement of the direct beam on the detector and an upstream monitor. After normalisation the data were reduced to normalized intensity vs. q by diffraction focusing [22], using the Mantid framework [23]. This culminated in a q range of 0.032 to 0.991 nm^{-1}.

A custom made hydration chamber was utilized to ensure the samples remained fully hydrated throughout the measurement. Samples were measured for 160–200 μAmp h of accelerator proton charge (~4–5 h) at 25 °C at each hydration depending on the signal to noise ratio. Scattered data were background subtracted using the Mantid software and the peaks fitted using the Fityk software, a software that offers more control for overlapping peak fitting [21].

2.5.3. Measurement at D16

The lipid arrangement measurements when 25% of the CER NS was substituted with FFA C24 and C18 (25% FFA sub) were performed on the D16 neutron diffractometer at the Institut Laue-Langevin (Grenoble, France). The measurement and data analysis procedure have been described previously [11,18,24]. In brief, the incoming slit-collimated beam (wavelength 4.49 Å) was set to 30.2 mm vertically and 3.0 mm horizontally. The diffraction patterns were measured in reflection mode, with the sample positioned 0.955 m from the 320 × 320 mm ^{3}He detector with a spatial resolution of 1 × 1 mm. Each samples were mounted in an aluminium humidity chamber [25], maintained at 25 °C and measured for a total of 5 to 6 h depending on the signal to noise ratio. Samples were rotated (Ω) between 0.05 and 10.2° at detector angle (γ) 11° (Ω = 0.05–2.25°) and 12° (Ω =1.8–10.2°), at 0.05° steps to cover the

first 9 diffraction orders. For each diffraction order, the scans measured at the specular angle and ± 0.1° (culminating to a total of 5 Ω steps), were averaged together and fitted. The scattering data were reduced, background subtracted, and the peaks fitted using the data processing software LAMP [26], peaks were fitted using Fityk.

While converting the data from scattering angle (2θ) into q-spacing, a rearranged Bragg equation was used;

$$q = (4\pi \sin\theta)/\lambda \tag{1}$$

When in the lamellar phase, a series of peaks at equal q-distances to one another are detected, and the repeat distance (d) of the lamellar phase can be calculated from the positions of the peaks as.

$$d = 2n\pi/q_n \tag{2}$$

with n as the order number of the diffraction peak located at position q_n.

2.5.4. Scattering length density calculations

Using the intensity vs q curves, the scattering length density (SLD) profile can be calculated. This method has been described previously [18,24,27]. In brief, diffraction orders were fitted with a Pearson7 function, in Fityk, to determine the scattering intensity (I). The structure factor amplitude ($|F_n|$) for each order was calculated as:

$$|F_n| = A_n \sqrt{LI} \tag{3}$$

and due to the high degree of orientation in the sample, the Lorentz correction (L) can be calculated as L = n. A_n is the correction factor for sample absorption, which is calculated [28] as:

$$A_n = \frac{1}{\sqrt{\frac{\sin\theta}{2\mu l}\left(1 - e^{\frac{-2\mu l}{\sin\theta}}\right)}} \tag{4}$$

where μ refers to the linear attenuation coefficient, and l is the sample thickness.

Due to the lost phase sign, typical of diffraction experiments, the phases need to be determined. The LPP has been identified as centrosymmetric in previous work [11]. This is shown by the linear variation of the structure factors (F_n) as a function of the D_2O:H_2O ratio (varied as 100:0, 50:50 and 8:92) (see Figs. S1 & S2 for the results obtained for the protiated and deuterated samples, respectively). To calculate the SLD profile of water in the LPP unit cell, the F_n of the sample hydrated at 8:92 D_2O:H_2O was subtracted from the sample hydrated at 100:0 D_2O:H_2O. The correct phase determination was identified by the water molecules located primarily at the unit cell boundary at the same position as the head groups. For calculating the SLD profile of water, the phase signs for the first 9 diffraction orders of the non-deuterated LPP sample were assigned as −,+,−,+,−,+,−,+,−. This combination locates the water molecules at the expected unit cell border, and with a second maximum at approximately 2.1 nm from the unit cell centre. These phase signs match with those previously reported for water in the LPP [11,24,27].

Using the F_n value, the SLD profile across the unit cell ($\rho(x)$) was calculated by Fourier reconstruction:

$$\rho(x) = F_0 + 2\sum_{n=1}^{n_{max}} \left(F_n \cos\frac{2\pi nx}{d} \right) \tag{5}$$

where x is the unit cell co-ordinate measured in the direction normal to the lamellar surface, and $x = 0$ is taken as the centre of the unit cell. The amplitude of the zero order structure factor (F_0) is equal to the scattering length density per unit volume of the sample and is calculated for each composition [29].

In order to determine the signs of the phases to calculate the SLD profiles for the various lipidic components of the LPP, the phase signs of the F_n at 8:92 D_2O:H_2O were determined with reference to Figs. S1 and S2. The reason for the use of 8:92 D_2O:H_2O hydrated sample is that at this level, the net contribution from the water is negligible. For the non-

deuterated, the 25% FFA sub model with d-FFA-C18, and the sphingo-sub model with sphingo-D7 compositions, the phase signs were determined as −,+,−,+,−,+,−,+,−. For the samples involving the 25% Sphingo-sub model with deuterated CER NS-D7 and CER NS-d47, the phase signs were determined as −,−,−,+,−,+ and +,+,−,+,−,+, respectively. For the 25%FFA-sub model, the phase signs for CER NS-D7 and CER NS-D47 were obtained as −,−,−,+,−,+,−,+,− and +,+,−,+,−,+,+,+,−, respectively.

To identify the location of the deuterated moieties of the lipids, the 8% $D_2O:H_2O$ SLD profile on the non-deuterated SLD profiles was subtracted from the 8% $D_2O:H_2O$ SLD profile containing the deuterated material, leaving only the scattering due to the deuterated moiety.

The 'relative absolute' scale was then calculated by determining the scaling factor from the difference in the scattering area between the protiated and deuterated profiles [11,30,31]. A description on

converting to relative absolute scale has been previously provided [18]. In short, the peak height (SLD_{height}) and area (SLD_{area}) for a deuterated peak in the SLD profile are determined and the corrected height is calculated as the difference in the scattering length densities of the protiated and deuterated versions (SLD_{diff}). In this study, we used the CER NS d7 peaks as it is the most defined of the peaks that we measured in both of our diffraction measurements. The correction is calculated as

$$SLD_{corrected} = \frac{SLD_{height} * SLD_{diff}}{SLD_{area}} \qquad (6)$$

Using the $SLD_{corrected}$ value the scaling factor can be determined by dividing with SLD_{height}.
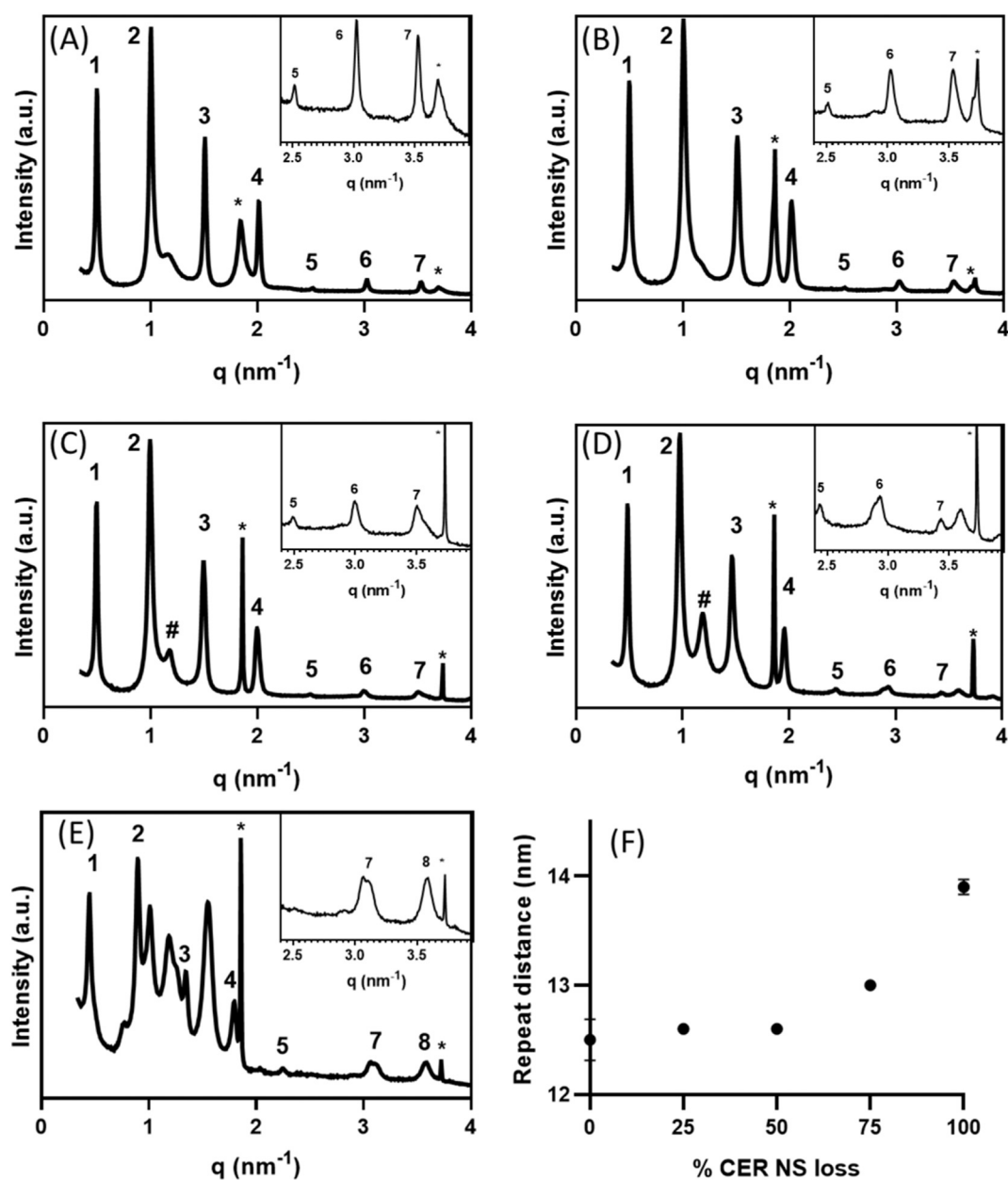

Fig. 2. SAXD curves of samples with (A) 0, (B) 25, (C) 50, (D) 75 and (E) 100% CER NS substitution with FFA C24 and free sphingosine. Samples were measured at 23 °C. The Arabic numbers indicate the LPP diffraction orders. * indicates the crystalline CHOL orders and # indicates the unknown peak at 1.18 nm^{-1}. All additional peaks are attributed to the phase separated structures. Inset: An enhanced image of curves between 2.4 and 4 nm^{-1}. (F) LPP repeat distance against the amount of CER NS substitution with FFA C24 and free sphingosine. Error is calculated as the standard deviation between the repeat measurements.

3. Results

3.1. The effect of increasing chain separation

To determine the effect of CER amide bond loss on the LPP lamellar formation, CER NS was substituted with a free sphingosine (C18) and a FFA C24 (the Sphingo-sub models) and measured with SAXD. The degree of substitution varied between 25% and 100%. The SAXD curves (Fig. 2A–E) show that a long periodicity phase remained for all CER NS concentrations measured, with the repeat distance increasing from 12.5 ± 0.2 nm, 12.6 ± 0.05 nm, 12.6 ± 0.05 nm, 13.0 ± 0.0 nm, and 13.9 ± 0.05 nm when 0, 25, 50, 75 and 100% of the CER NS was substituted, respectively (Fig. 2F). At 0% and 25% CER NS substitution, the LPP and crystalline CHOL were the only lipid structures that formed. As CER NS concentration decreased to 50% of the original content, a peak at 1.18 nm^{-1} (d = 5.3 nm) is visible. A similar profile is seen at 75% CER NS

substitution, with a stronger peak at 1.18 nm^{-1} (Fig. 2D, #), indicating that a larger proportion of the lipids are forming the new structure in the sample. When 100% of the CER NS is substituted, many additional peaks were present (Fig. 2E). When the CER NS concentration is reduced within the sample, the peak intensity of the crystalline CHOL (*) increases, implying a higher fraction of phase separated CHOL. This may be attributed to the decreased fraction of lipids forming the longer periodicity phase in the samples. At 100% substitution, the 13.9 nm repeat distance is long, which implies that it may no longer be an LPP.

SAXD measurements were also performed on the FFA-sub models, where the CER NS is substituted with a FFA C18 and FFA C24 molecule. Here the component acyl chains of the CER NS are replaced by the free species and the characteristic sphingosine head group is removed which will thus affect the headgroup interactions within the lamellae. Fig. 3A–D shows the SAXD curves for samples where 25, 50, 75 and 100% of the CER NS is substituted resulting in repeat distances of 12.5 ±
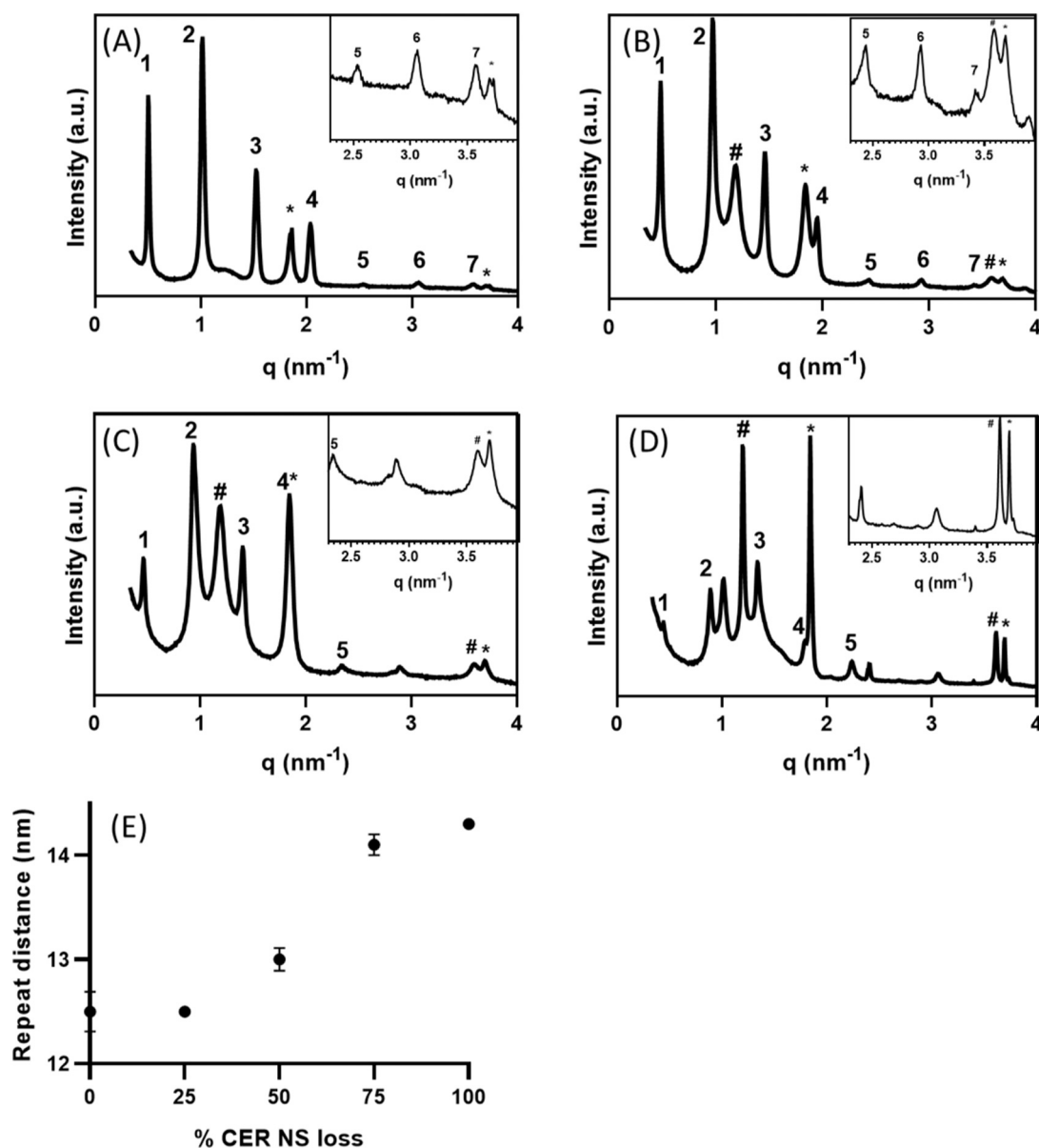

Fig. 3. SAXS curves of hydrated samples with (A) 25, (B) 50, (C) 75 and (D) 100% CER NS substitution with FFA C24 and C18. Samples were measured at 23 °C. The Arabic numbers indicate the LPP diffraction orders. * indicates the crystalline CHOL order, and # indicates the additional unknown phase with an initial peak at approximately 1.18 nm^{-1}. All additional peaks are attributed to the phase separated structures. Insert: an enhanced image of curves between 2.2 and 4 nm^{-1}. (E) LPP repeat distance against the amount of CER NS substitution with FFA C24 and FFA C18. Error is calculated as the standard deviation between the repeat measurements.

0.05 nm, 13.0 ± 0.1 nm, 14.1 ± 0.1 nm, and 14.3 ± 0.05 nm, respectively (Fig. 3E). Similar to the sphingosine-substituted models, only the LPP and crystalline CHOL had formed at 0% and 25% CER NS substitution. When increased to 50% and 75% substitution, a structure with a first order located at 1.18 nm^{-1} is present (# in Fig. 3C). Fig. 3C shows that the CHOL and 4th order LPP peak overlap in the 75% FFA-sub model. When 100% of the CER NS was replaced, the repeat distance is longer and the repeat peak intensities are significantly changed, implying that the longer phase is no longer an LPP. Moreover, there are additional peaks seen, suggesting that additional phases have formed, after the loss of all the CER NS in the model. As with the Sphingo-sub models, when more of the CER NS is substituted, the amount of CHOL that is phase separated as crystalline CHOL increases, (as indicated by the relative increase in intensity of the crystalline CHOL peaks, Fig. 3A–D,*). An alternative explanation would be that at 100% substitution the LPP is no longer formed and that a longer periodicity structure is formed instead – as seen in samples prepared with CER EOS [32,33].

3.2. No changes in the lateral packing and conformational ordering after the substitutional loss of CER NS

SAXD data showed phase separation occurring at ≥50% CER NS substitution. To further investigate the apparent indifference when 25% of CER NS was substituted with FFA C24 and either sphingosine or FFA C18, the conformational ordering and lateral lipid organization were examined with FTIR spectroscopy. The conformational ordering is determined by the position of the CH$_2$ symmetric stretching mode (νCH$_2$, 2845–2855 nm^{-1}), and the thermotropic response for the 0% sub model is presented in Fig. 4A. The thermotropic response curves for the 0% sub, 25% Sphingo-sub and the 25% FFA-sub samples were similar as shown in Fig. S3, and at 24 °C the νCH$_2$ were similar with values of 2848.9, 2848.7 and 2848.7 cm^{-1} respectively, the lower wavenumber values indicating highly ordered chains. As the temperature was increased the average hexagonal phase mid-transition temperature for the three models remained similar at 40.2 ± 1.0, 37.5 ± 0.6, and 39.4 ± 1.1 °C for the 0% sub, 25% Sphingo-sub and the 25% FFA-sub, respectively. Further heating showed that the fluid phase mid-transition was also similar between the models at temperatures of 69.9 ± 1.5, 69.8 ± 0.8, and 70.7 ± 0.6 °C, respectively. Comparing the behaviour of the 25% Sphingo-sub and 25% FFA-sub samples, the substitution had no noticeable effect on the lipid conformational ordering behaviour. The orthorhombic domain size and inter-chain interaction can be probed by the splitting in the CH$_2$ scissoring mode (δCH$_2$, 1460 to 1480 cm^{-1})

peaks. Fig. 4B shows that the peak maxima at 1462 and 1473 cm^{-1} did not shift and that the peak shape did not change, implying there was no significant difference in the lateral packing between the 0, 25% Sphingo-sub and 25% FFA-sub samples.

3.3. Head group moiety dictates the location of the lipids within the LPP

To further probe if there was any change in the LPP structure in the 25% Sphingo-sub and 25% FFA-sub models, the lipid arrangement in the unit cell of the LPP was investigated with SANS. Similar to the SAXD curves, the intensity vs q curves for all models demonstrated that the only lamellar structure present was the LPP, with the only additional structure being phase separated crystalline CHOL. The repeat distances were determined by least square fitting of all peak positions. The mean repeat distance determined for the 25% Sphingo-sub model was 12.6 ± 0.1 nm, while the mean repeat distance for the 25% FFA-sub model was 12.6 ± 0.1 nm.

To determine the structure of the LPP, the water profile was determined by subtracting the SLD profile intensity, in relation to the position within the unit cell (x), when hydrated with a solvent of 100:0 D$_2$O:H$_2$O, from the SLD profile intensity calculated when hydrated in a 8:92 D$_2$O: H$_2$O solvent. Fig. 5A shows the water to be located at the unit cell boundary at 2.2 nm from the centre of the unit cell, demonstrating the characteristic trilayer structure of the LPP. To determine whether a rearrangement of the lipids had occurred as a result of the substitution of some of the CER NS, each of the chains of the remaining CER NS fraction had either the sphingosine chain or the acyl chain deuterated to provide both positional and conformational information (hairpin versus linear conformation). The location of the deuterated chains was determined by the subtraction of the SLD profile for the non-deuterated sample from that of the profile for the sample involving deuterated lipid, both hydrated in 8% D$_2$O solvent.

First, we present the 25% Sphingo-sub model. The green curve in Fig. 5B shows that the peak corresponding to the terminal d7 moiety of the sphingosine chain of the CER NS (CER NS-d7) is located exclusively at 4.6 nm from the centre of the LPP. The peak for the deuterated acyl chain of CER NS, shows that this is primarily located in the centre of the unit cell (Fig. 5B, red curve). This indicates that the CER NS is arranged in a linear fashion with the CER headgroup located primarily at the inner water region. In this case, the acyl chains are located at the centre of the unit cell, while the sphingosine chain of the CER NS is extended to the outer layers of the LPP. The location of the free sphingosine chain was also determined using sphingosine-d7. The loci of the terminal carbons of the free sphingosine-d7 (Fig. 5A, black curve), are positioned at 4.6
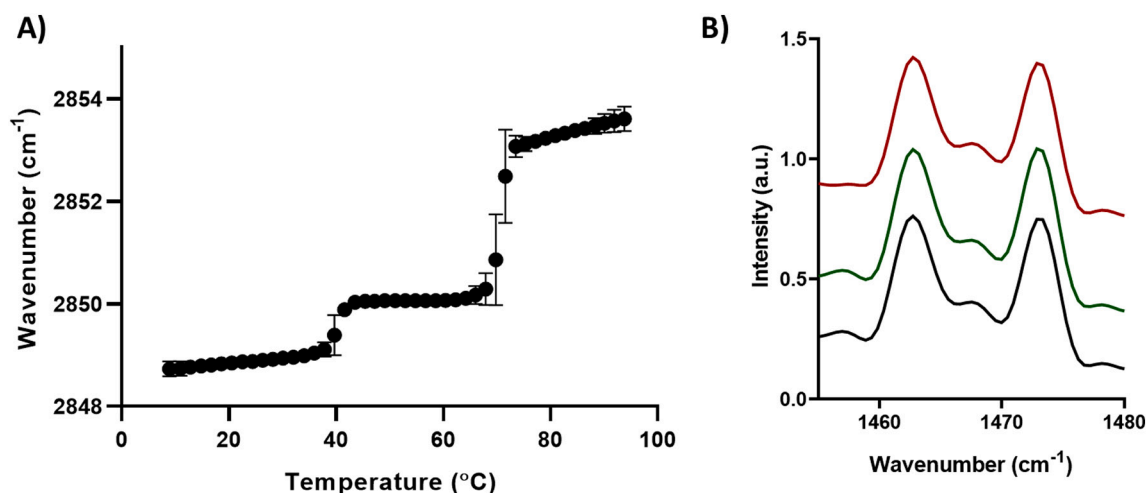

Fig. 4. A) νCH$_2$ thermotropic response curve for 0% sub model. The mean value is presented, the error is calculated as the standard deviation. B) δCH$_2$ curves for 0% sub (black), 25% Sphingo-sub (green), and 25% FFA-sub (red) models at 20 °C, no difference is visible between the models.
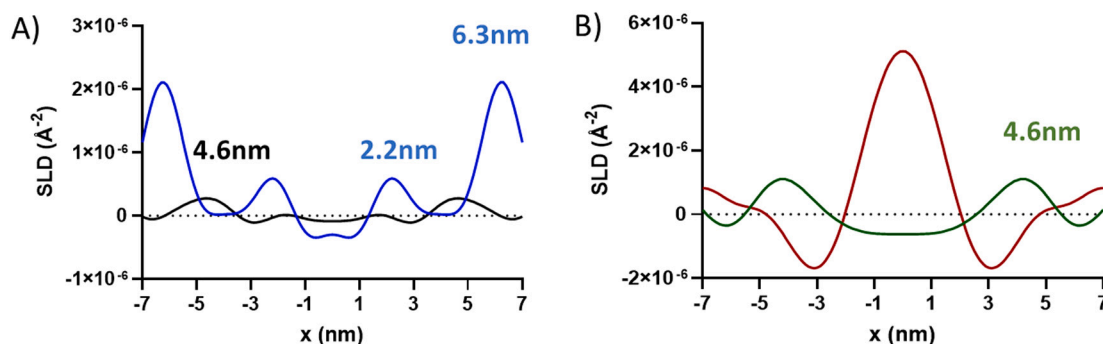
Fig. 5. SLD profile of 25% Sphingo-sub, where CER NS is substituted with FFA C24 and free sphingosine. A) The water profile, indicating the position of the water molecules (blue), and the terminal position of the free sphingosine (d7, black). B) The terminal position of the CER NS's sphingosine chain (d7, green), and the length of the acyl chain (d47, red).

nm from the unit cell centre, and a similar position is found for the CER NS-d7 sphingosine chain, albeit that the peak intensity is lower in this case due to the lower degree of deuteration.

The LPP mean repeat distance of the 25% FFA-sub model was 12.6 ± 0.1 nm, and aside from phase separated crystalline CHOL, was the only lamellar structure present in the system. Fig. 6 shows the SLD profiles for the LPP having this lipid composition. Similar to Fig. 5, Fig. 6A (blue) shows the water to be located at the unit cell boundary at 2.1 nm from the cell centre. The position of the terminal sphingosine chain of CER NS-d7 is located 4.2 nm from the centre of the LPP unit cell, while the acyl chain of CER NS-d47 is more evenly distributed between the central and outer lipid layers of the unit cell than in the 25% Sphingo-sub model. These positions imply that the CER NS in the centre remains in an extended conformation while a larger proportion of the CER NS has migrated to the outer regions when compared to the 25% Sphingo-sub model (see Fig. 5B). It is not known whether the CER NS in the outer region is in an extended or hairpin conformation. The SLD profile of the free FFA C18 shows no regions of higher SLD intensity throughout the unit cell implying the FFA C18 is distributed evenly throughout.

4. Discussion

4.1. The importance of sphingosine headgroup for lipid arrangement

Our results show that with decreasing levels of CER NS, an increasing fraction of the lipids does not form the LPP. However, this did not occur when 25% of CER NS was substituted suggesting below this level the LPP structure remains insensitive to the CER NS loss. In the 25% Sphingo-sub model, the CER NS is primarily arranged with the headgroup in the inner headgroup region with its acyl chain in the central alkyl chain layer and the sphingosine chain in the outer alkyl layers. The free sphingosine acyl chain tail end was also located in the outer alkyl chain layer of the LPP.

This implies that the sphingosine headgroup can be located either in the inner or outer head group regions. However, as most of the CER NS is in the inner head group region, the sphingosine headgroup is most likely located in the outer headgroup region located at the unit cell boundary. This change in lipid arrangement is shown in Fig. 7.

In the 25% FFA-sub model, where 25% of the CER NS was substituted with FFA C24 and C18, a difference in the LPP lipid arrangement was observed. This included a redistribution of CER NS, wherein the acyl chains are located at both the inner and outer bilayers of the LPP when compared to the other model that had a strong bias for the CER NS head group being located in the headgroup region with the acyl chain in the inner lipid layer of the LPP. It was also observed that the FFA C18 is equally distributed throughout the LPP in contrast to the free sphingosine in the 25% Sphingo-sub model that remained in the outer layers of the LPP. The change in lipid arrangement it presented in Fig. 7.

In terms of the location and conformation of CER NS in an equimolar lipid class ratio of 1:1:1 CER:CHOL:FFA (with 40% CER EOS and 60% CER NS in the CER mixture), the CER NS headgroup has previously been reported to be located within the inner head group region and to a lesser extent at the unit cell boundary of the LPP [18,24]. In the central headgroup region, the CER NS is exclusively in an extended conformation, and this was also seen in the 25% Sphingo-sub and 25% FFA-sub models.

Our results show that the sphingosine head group plays a crucial role in directing the sphingosine carbon chains into the outer head group regions, and when free sphingosine is still present CER NS does not have to compensate. However, when the sphingosine moiety is replaced by a fatty acid, CER NS needs to compensate and distributes more homogeneously in the LPP unit cell. CER head groups are known to have a significant effect on the LPP and SPP behaviour, and this includes an influences on the packing density, lipid miscibility, and hydrogen bonding strength [20,34,35]. To our knowledge, no studies have
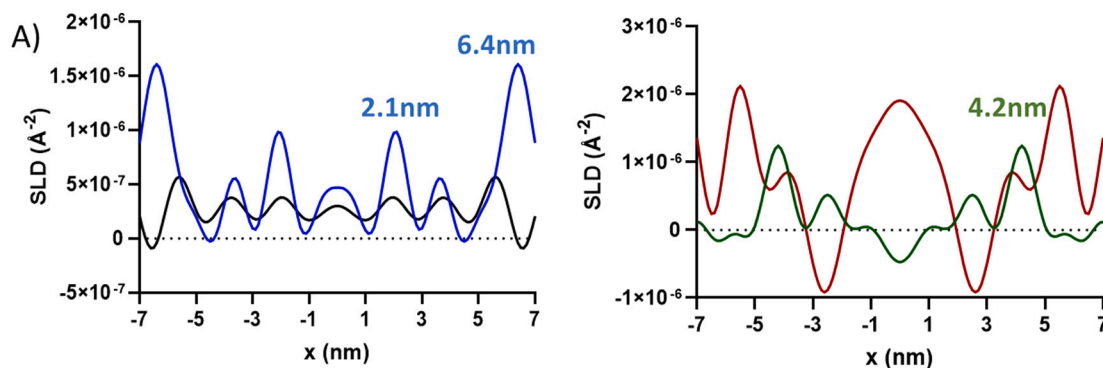

Fig. 6. SLD profile of 25% FFA-sub, where 25% of CER NS is substituted with a FFA C24 and FFA C18. A) The water profile (blue) and the position of the entire carbon chain of the FFA C18 (black). B) The terminal position of the CER NS's sphingosine chain (d7, green), and the length of the acyl chain (d47, red).
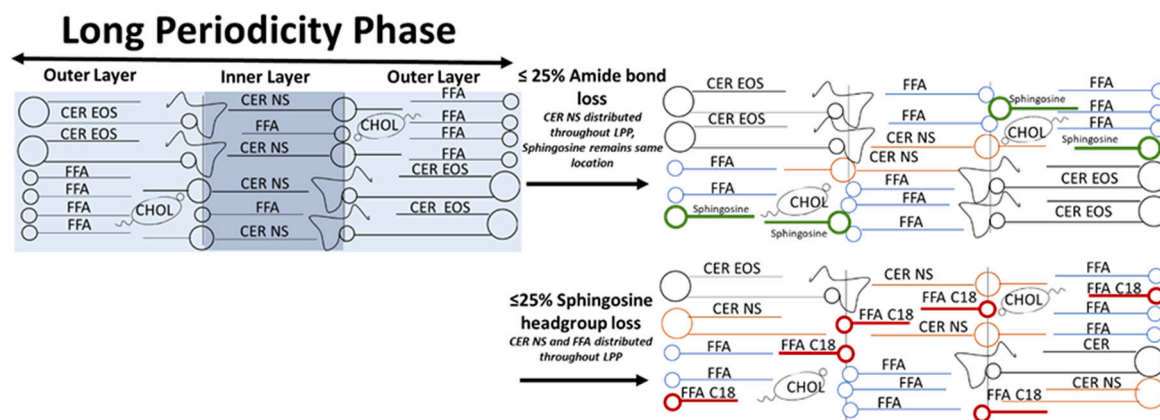
Fig. 7. Schematic diagram of the lipid arrangement of the LPP both unmodified (left) and when under ≤25% Amide bond loss, with the substitution of sphingosine (green) and FFA C24 (blue) with CER NS (top right). Or ≤25% Sphingosine headgroup loss, with the substitution of FFA C18 (red) and FFA C24 (blue) with CER NS (bottom right).

previously reported the importance of the CER headgroup for lipid localization in the LPP.

4.2. The importance of separating headgroup and carbon chain effect on the LPP

In the 25% Sphingo-sub and 25% FFA-sub models, neither the lamellar organization nor lateral packing of the system were altered when compared to previously reported LPP structures [11]. During this study, we have ensured that the carbon chain length distribution remained the same for all the samples. Ordinarily, the carbon chain's van der Waal interactions have a strong stabilizing effect, particularly for skin lipids that contain long average chain lengths and this may explain the results obtained here. Carbon chain length effects on SC lamellar structures are important, and when the normal chain length composition is reduced, this can cause a range of effects including; an increased conformational disordering and lipid mobility [36], induced phase separation [37–40], reduced lipid density [41], and as a consequence an increased trans-epidermal water loss and thus a reduction in skin barrier [42,43]. In comparison, the small loss in headgroup interactions due to the decrease in the CER NS fraction is not sufficient to influence the lipid arrangement.

4.3. CER intermediates in diseased skin may be underrepresented

The organization of the lipid matrix of the SC is essential for the skin's barrier function. One common alteration found in diseased skin is an overall loss of CER concentration, which varies in severity. Reduced activity of ceramide synthases or an increase in ceramidase activity are underlying factors for the decrease in CER content and an increase in free sphingosine. While other synthetic pathway alterations that may also reduce CER content include a reduced activity of Glucocerebrosidase [44] and Sphingomyelinase [45]. In these cases, the reduced production of CERs, which again results in the reduction of the overall concentration of CER, can increase the overall concentration of CER precursors. LC-MS is often used to determine the lipid composition of SC [46]. Typical LC-MS measurements can identify the CHOL, CER subclass (headgroup) and the carbon chain length of both CERs and FFAs. However, CER intermediates such as free sphingosine are also present in the skin [47] and can be easily overlooked since the methods particularly developed for CER analysis are often not optimal for the detection of sphingosines [48,49]. This difficulty to detect sphingosine and other intermediate structures may explain the limited reports on this area. However, Toncic et al. [50] have identified an increase in the level of free sphingosine within the skin in patients with atopic dermatitis, partially within lesional skin.

The observed mixed phases at substitutions of CER concentrations >25%, could be a mechanism of expelling the excessive amount of FFAs. This reduces the ratio found in the long periodicity phase, back to a similar value to before the substitution had occurred, to best accommodate for the LPP. However, this mechanism appears only to be valid up to a certain degree of substitution, and the structure can no longer be maintained once the substitution exceeds a certain level as seen in our 100% sub samples.

5. Conclusions

The behaviour and structure of the SC lipid matrix are dependent on the lipid composition. Our results indicate that the presence of the sphingosine head group is important to have a similar distribution of CER NS compared to equimolar lipid models. However, there is still no change in lipid organization until 25%. Thus, our results indicate that an increased ceramidase activity or reduced ceramide synthase activity, does not lead to dramatic changes in the lipid phase behaviour of the ceramides as the free sphingosine would partially play the role of CER NS concerning its location.

It was not until the sphingosine head group was removed that its importance in the CER NS localization and the need for the sphingosine head group at the boundary of the LPP unit cell was identified. With a strong increase in both short and long chain FFA concentration, a redistribution of CERs in the LPP may occur, and this is likely relevant for FFA rich skin diseases.

Declaration of competing interest

The authors declare that they have no known competing financial interests or personal relationships that could have appeared to influence the work reported in this paper.

Appendix A. Supplementary data

Supplementary data to this article can be found online at https://doi.org/10.1016/j.bbamem.2022.183886.

References

[1] E. Proksch, J.M. Brandner, J.M. Jensen, The skin: an indispensable barrier, Exp. Dermatol. 17 (2008) 1063–1072.

[2] P.M. Elias, Epidermal barrier function: intercellular lamellar lipid structures, origin, composition and metabolism, J. Control. Release 15 (1991) 199–208.

[3] P.S. Talreja, G.B. Kasting, N.K. Kleene, W.L. Pickens, T.F. Wang, Visualization of the lipid barrier and measurement of lipid pathlength in human stratum corneum, AAPS PharmSci 3 (2001) 48–56.

[4] H.E. Boddé, M.A.M. Kruithof, J. Brussee, H.K. Koerten, Visualisation of normal and enhanced HgCl2 transport through human skin in vitro, Int. J. Pharm. 53 (1989) 13–24.

[5] J.A. Bouwstra, G.S. Gooris, W. Bras, D.T. Downing, Lipid organization in pig Stratum Corneum, J. Lipid Res. 36 (1995) 685–695.

[6] J.R. Hill, P.W. Wertz, Molecular models of the intercellular lipid lamellae from epidermal Stratum Corneum, Biochim. Biophys. Acta Biomembr. 1616 (2003) 121–126.

[7] S.H. White, D. Mirejovsky, G.I. King, Structure of lamellar lipid domains and corneocyte envelopes of murine Stratum Corneum. An X-ray diffraction study, Biochemistry 27 (1988) 3725–3732.

[8] F. Damien, M. Boncheva, The extent of orthorhombic lipid phases in the stratum corneum determines the barrier efficiency of human skin in vivo, J. Investig. Dermatol. 130 (2010) 611–614.

[9] M. Boncheva, F. Damien, V. Normand, Molecular organization of the lipid matrix in intact Stratum Corneum using ATR-FTIR spectroscopy, Biochim. Biophys. Acta Biomembr. 1778 (2008) 1344–1355.

[10] D. Groen, D.S. Poole, G.S. Gooris, J.A. Bouwstra, Is an orthorhombic lateral packing and a proper lamellar organization important for the skin barrier function? Biochim. Biophys. Acta Biomembr. 2011 (1808) 1529–1537.

[11] E.H. Mojumdar, G.S. Gooris, D. Groen, D.J. Barlow, M.J. Lawrence, B. Demé, J. A. Bouwstra, Stratum corneum lipid matrix: location of acyl ceramide and cholesterol in the unit cell of the long periodicity phase, Biochim. Biophys. Acta Biomembr. 1858 (2016) 1926–1934.

[12] K.R. Feingold, The outer frontier: the importance of lipid metabolism in the skin, J. Lipid Res. 50 (Suppl) (2009) S417–S422.

[13] E. Houben, J.P. Hachem, K. De Paepe, V. Rogiers, Epidermal ceramidase activity regulates epidermal desquamation via stratum corneum acidification, Skin Pharmacol. Physiol. 21 (2008) 111–118.

[14] K. Jin, Y. Higaki, Y. Takagi, K. Higuchi, Y. Yada, M. Kawashima, G. Imokawa, Analysis of beta-glucocerebrosidase and ceramidase activities in atopic and aged dry skin, Acta Derm. Venereol. 74 (1994) 337–340.

[15] Y. Ohnishi, N. Okino, M. Ito, S. Imayama, Ceramidase activity in bacterial skin flora as a possible cause of ceramide deficiency in atopic dermatitis, Clin. Diagn. Lab. Immunol. 6 (1999) 101–104.

[16] J. Arikawa, M. Ishibashi, M. Kawashima, Y. Takagi, Y. Ichikawa, G. Imokawa, Decreased levels of sphingosine, a natural antimicrobial agent, may be associated with vulnerability of the stratum corneum from patients with atopic dermatitis to colonization by Staphylococcus aureus, J. Investig. Dermatol. 119 (2002) 433–439.

[17] S. Motta, M. Monti, S. Sesana, R. Caputo, S. Carelli, R. Ghidoni, Ceramide composition of the psoriatic scale, Biochim. Biophys. Acta Mol. basis Dis. 1182 (1993) 147–151.

[18] C.M. Beddoes, G.S. Gooris, F. Foglia, D. Ahmadi, D.J. Barlow, M.J. Lawrence, B. Demé, J.A. Bouwstra, Arrangement of ceramides in the skin: sphingosine chains localize at a single position in stratum corneum lipid matrix models, Langmuir 36 (2020) 10270–10278.

[19] G.S. Gooris, M. Kamran, A. Kros, D.J. Moore, J.A. Bouwstra, Interactions of dipalmitoylphosphatidylcholine with ceramide-based mixtures, Biochim. Biophys. Acta Biomembr. 1860 (2018) 1272–1281.

[20] L.E. Uche, G.S. Gooris, C.M. Beddoes, J.A. Bouwstra, New insight into phase behavior and permeability of skin lipid models based on sphingosine and phytosphingosine ceramides, Biochim. Biophys. Acta Biomembr. 1861 (2019) 1317–1328.

[21] M. Wojdyr, Fityk: a general-purpose peak fitting program, J. Appl. Crystallogr. 43 (2010) 1126–1128.

[22] J.D. Jorgensen, J. Faber Jnr, J.M. Carpenter, R.K. Crawford, J.R. Haumann, R. L. Hitterman, R. Kleb, G.E. Ostrowski, F.J. Rotella, T.G. Worlton, Electronically focused time-of-flight powder diffractometers at the intense pulsed neutron source, J. Appl. Crystallogr. 22 (1989) 321–333.

[23] O. Arnold, J.C. Bilheux, J.M. Borreguero, A. Buts, S.I. Campbell, L. Chapon, M. Doucet, N. Draper, R.Ferraz Leal, M.A. Gigg, V.E. Lynch, A. Markvardsen, D. J. Mikkelson, R.L. Mikkelson, R. Miller, K. Palmen, P. Parker, G. Passos, T. G. Perring, P.F. Peterson, S. Ren, M.A. Reuter, A.T. Savici, J.W. Taylor, R.J. Taylor, R. Tolchenov, W. Zhou, J. Zikovsky, Mantid—data analysis and visualization package for neutron scattering and μ SR experiments, Nucl. Instrum. Methods Phys. Res., Sect. A 764 (2014) 156–166.

[24] E.H. Mojumdar, G.S. Gooris, D.J. Barlow, M.J. Lawrence, B. Demé, J.A. Bouwstra, Skin lipids: localization of ceramide and fatty acid in the unit cell of the long periodicity phase, Biophys. J. 108 (2015) 2670–2679.

[25] J. Gonthier, M.A. Barrett, O. Aguettaz, S. Baudoin, E. Bourgeat-Lami, B. Demé, N. Grimm, T. Hauß, K. Kiefer, E. Lelièvre-Berna, A. Perkins, D. Wallacher, BerILL: the ultimate humidity chamber for neutron scattering, J. Neutron Res. 21 (2019) 65–76.

[26] R. Didier, M. Ferrand, G.J. Kearley, Analysis and visualisation of neutron-scattering data, J. Neutron Res. 4 (1996) 33–39.

[27] D. Groen, G.S. Gooris, J.A. Bouwstra, New insights into the stratum corneum lipid organization by X-ray diffraction analysis, Biophys. J. 97 (2009) 2242–2249.

[28] N.P. Franks, W.R. Lieb, The structure of lipid bilayers and the effects of general anaesthetics: an X-ray and neutron diffraction study, J. Mol. Biol. 133 (1979) 469–500.

[29] T.A. Harroun, J. Katsaras, S.R. Wassall, Cholesterol hydroxyl group is found to reside in the center of a polyunsaturated lipid membrane, Biochemistry 45 (2006) 1227–1233.

[30] E.H. Mojumdar, D. Groen, G.S. Gooris, D.J. Barlow, M.J. Lawrence, B. Demé, J. A. Bouwstra, Localization of cholesterol and fatty acid in a model lipid membrane: a neutron diffraction approach, Biophys. J. 105 (2013) 911–918.

[31] M.C. Wiener, G.I. King, S.H. White, Structure of a fluid dioleoylphosphatidylcholine bilayer determined by joint refinement of x-ray and neutron diffraction data. I. Scaling of neutron data and the distributions of double bonds and water, Biophys. J. 60 (1991) 568–576.

[32] D. Groen, G.S. Gooris, J.A. Bouwstra, Model membranes prepared with ceramide EOS, cholesterol and free fatty acids form a unique lamellar phase, Langmuir 26 (2010) 4168–4175.

[33] L.E. Uche, G.S. Gooris, J.A. Bouwstra, C.M. Beddoes, High concentration of the ester-linked ω-hydroxy ceramide increases the permeability in skin lipid model membranes, Biochim. Biophys. Acta Biomembr. 1863 (2021), 183487.

[34] B. Školová, A. Kováčik, O. Tesař, L. Opálka, K. Vávrová, Phytosphingosine, sphingosine and dihydrosphingosine ceramides in model skin lipid membranes: permeability and biophysics, Biochim. Biophys. Acta Biomembr. 1859 (2017) 824–834.

[35] M.E. Rerek, D. Van Wyck, R. Mendelsohn, D.J. Moore, FTIR spectroscopic studies of lipid dynamics in phytosphingosine ceramide models of the stratum corneum lipid matrix, Chem. Phys. Lipids 134 (2005) 51–58.

[36] M. Uchiyama, M. Oguri, E.H. Mojumdar, G.S. Gooris, J.A. Bouwstra, Free fatty acids chain length distribution affects the permeability of skin lipid model membranes, Biochim. Biophys. Acta Biomembr. 2016 (1858) 2050–2059.

[37] B. Školová, K. Hudská, P. Pullmannová, A. Kováčik, K. Palát, J. Roh, J. Fleddermann, I. Estrela-Lopis, K. Vávrová, Different phase behavior and packing of ceramides with long (C16) and very long (C24) acyls in model membranes: infrared spectroscopy using deuterated lipids, J. Phys. Chem. B 118 (2014) 10460–10470.

[38] P. Pullmannová, L. Pavlíková, A. Kováčik, M. Sochorová, B. Školová, P. Slepička, J. Maixner, J. Zbytovská, K. Vávrová, Permeability and microstructure of model stratum corneum lipid membranes containing ceramides with long (C16) and very long (C24) acyl chains, Biophys. Chem. 224 (2017) 20–31.

[39] A. Paz Ramos, M. Lafleur, Chain length of free fatty acids influences the phase behavior of stratum corneum model membranes, Langmuir 31 (2015) 11621–11629.

[40] M. Oguri, G.S. Gooris, K. Bito, J.A. Bouwstra, The effect of the chain length distribution of free fatty acids on the mixing properties of stratum corneum model membranes, Biochim. Biophys. Acta Biomembr. 2014 (1838) 1851–1861.

[41] B. Janůšová, J. Zbytovská, P. Lorenc, H. Vavrysová, K. Palát, A. Hrabálek, K. Vávrová, Effect of ceramide acyl chain length on skin permeability and thermotropic phase behavior of model stratum corneum lipid membranes, Biochim. Biophys. Acta Mol. Cell Biol. Lipids 1811 (2011) 129–137.

[42] J. Ishikawa, H. Narita, N. Kondo, M. Hotta, Y. Takagi, Y. Masukawa, T. Kitahara, Y. Takema, S. Koyano, S. Yamazaki, A. Hatamochi, Changes in the ceramide profile of atopic dermatitis patients, J. Investig. Dermatol. 130 (2010) 2511–2514.

[43] M. Janssens, J. van Smeden, G.S. Gooris, W. Bras, G. Portale, P.J. Caspers, R. J. Vreeken, T. Hankemeier, S. Kezic, R. Wolterbeek, A.P. Lavrijsen, J.A. Bouwstra, Increase in short-chain ceramides correlates with an altered lipid organization and decreased barrier function in atopic eczema patients, J. Lipid Res. 53 (2012) 2755–2766.

[44] S. Hamanaka, A. Suzuki, M. Hara, H. Nishio, F. Otsuka, Y. Uchida, Human epidermal glucosylceramides are major precursors of stratum corneum ceramides, J. Investig. Dermatol. 119 (2002) 416–423.

[45] J.-M. Jensen, R. Fölster-Holst, A. Baranowsky, M. Schunck, S. Winoto-Morbach, C. Neumann, S. Schütze, E. Proksch, Impaired sphingomyelinase activity and epidermal differentiation in atopic dermatitis, J. Investig. Dermatol. 122 (2004) 1423–1431.

[46] J. van Smeden, W.A. Boiten, T. Hankemeier, R. Rissmann, J.A. Bouwstra, R. J. Vreeken, Combined LC/MS-platform for analysis of all major stratum corneum lipids, and the profiling of skin substitutes, Biochim. Biophys. Acta Mol. Cell Biol. Lipids 1841 (2014) 70–79.

[47] P.W. Wertz, D.T. Downing, Free sphingosine in human epidermis, J. Investig. Dermatol. 94 (1990) 159–161.

[48] W. Boiten, S. Absalah, R. Vreeken, J. Bouwstra, J. van Smeden, Quantitative analysis of ceramides using a novel lipidomics approach with three dimensional response modelling, Biochim. Biophys. Acta Mol. Cell Biol. Lipids 1861 (2016) 1652–1661.

[49] Y. Masukawa, H. Narita, H. Sato, A. Naoe, N. Kondo, Y. Sugai, T. Oba, R. Homma, J. Ishikawa, Y. Takagi, Comprehensive quantification of ceramide species in human stratum corneum, J. Lipid Res. 50 (2009) 1708–1719.

[50] R.J. Toncic, I. Jakasa, S.L. Hadzavdic, S.M. Goorden, K.J. Vlugt, F.S. Stet, A. Balic, M. Petkovic, B. Pavicic, K. Zuzul, B. Marinovic, S. Kezic, Altered levels of sphingosine, sphinganine and their ceramides in atopic dermatitis are related to skin barrier function, disease severity and local cytokine milieu, Int. J. Mol. Sci. 21 (2020).